The C-terminal tail domain of metavinculin, vinculin's splice variant, severs actin filaments

Mandy E.W. Janssen, HongJun Liu, Niels Volkmann, and Dorit Hanein

Bioinformatics and Systems Biology Program, Sanford–Burnham Medical Research Institute, La Jolla, CA 92037

Vinculin and its splice variant, metavinculin (MV), are key elements of multiple protein assemblies linking the extracellular matrix to the actin cytoskeleton. Vinculin is expressed ubiquitously, whereas MV is mainly expressed in smooth and cardiac muscle tissue. The only difference in amino acid sequence between the isoforms is a 68-residue insert in the C-terminal tail domain of MV (MVt). Although the functional role of this insert remains elusive, its importance is exemplified by point mutations that are associated with dilated and hypertrophic cardiomyopathy. In vinculin, the actin binding site resides in the tail domain. In this paper, we show that MVt binds actin filaments similarly to the vinculin tail domain. Unlike its splice variant, MVt did not bundle actin filaments. Instead, MVt promoted severing of actin filaments, most efficiently at substoichiometric concentrations. This surprising and seemingly contradictory alteration of vinculin function by the 68-residue insert may be essential for modulating compliance of vinculin-induced actin bundles when exposed to rapidly increasing external forces.

Introduction

Vinculin is a highly conserved 116-kD protein, which links actin filaments to the cell membrane via cadherins and integrins in cell–cell and cell–matrix adhesion junctions, respectively. It plays a crucial role in brain and heart development, in which it is required for the formation of normal cell–cell and cell–matrix adhesive complexes (Xu et al., 1998; Zemljic-Harpf et al., 2007).Vinculin interacts with a large number of proteins (Ziegler et al., 2006), but most of its binding sites are masked by an intermolecular interaction between the vinculin head and tail domain, which renders the protein inactive (Bakolitsa et al., 2004; Borgon et al., 2004). It was proposed that binding of talin to the vinculin head domain and a subsequent helical bundle conversion are sufficient to activate vinculin (Izard et al., 2004). A combinatorial activation mechanism was also proposed in which vinculin is activated by simultaneous binding of two or more of its ligands (Bakolitsa et al., 2004; Janssen et al., 2006). Recent molecular dynamics investigations further support the latter (Golji and Mofrad, 2010).

The existence of a vinculin splice variant, metavinculin (MV), was recognized nearly three decades ago (Feramisco et al., 1982). Although extensive research has been performed on vinculin, the function of its larger isoform remains elusive. Vinculin is expressed ubiquitously, whereas MV is mainly expressed in smooth and cardiac muscle tissue (Feramisco et al., 1982; Glukhova et al., 1986; Belkin et al., 1988). A minor fraction of MV can also be found in skeletal muscle tissue and platelets (Turner and Burridge, 1989). The ratio of the two isoforms depends on tissue type and ranges between 1:1 and 4:1 for vinculin/MV (Belkin et al., 1988). MV expression appears to be directly correlated to the ability of differentiated muscle cells to contract (Saga et al., 1985; Koteliansky et al., 1991), suggesting that MV is important for force transduction.

The sole difference between the two isoforms in humans is a 68-residue acidic insert in MV that is located between residues 915 and 916 of vinculin, a loop between the first two helices (H1 and H2) of the C-terminal tail domain (Vt; Gimona et al., 1988; Byrne et al., 1992). In both isoforms, the actin binding site resides in the respective tail domain and is masked by the head domain in the full-length molecule (Fig. 1, B and C). Vt forms a five-helix bundle, H1–H5 (Bakolitsa et al., 1999), with the actin binding site primarily residing in H3, H4, and the C terminus (Janssen et al., 2006). A helix formed by the C-terminal part of the MV insert (H1′, residues 964–979) replaces H1 in Vt to form a new, but structurally similar, five-helix bundle (Rangarajan et al., 2010). The ordered "strap" region

Correspondence to Neils Volkmann: niels@burnham.org; or Dorit Hanein: dorit@burnham.org

M.E.W. Janssen's present address is The Scripps Research Institute, La Jolla, CA 92037.

Abbreviations used in this paper: FSC, Fourier shell correlation; MV, metavinculin.

The Rockefeller University Press $30.00
J. Cell Biol. Vol. 197 No. 5 585–593
www.jcb.org/cgi/doi/10.1083/jcb.201111046

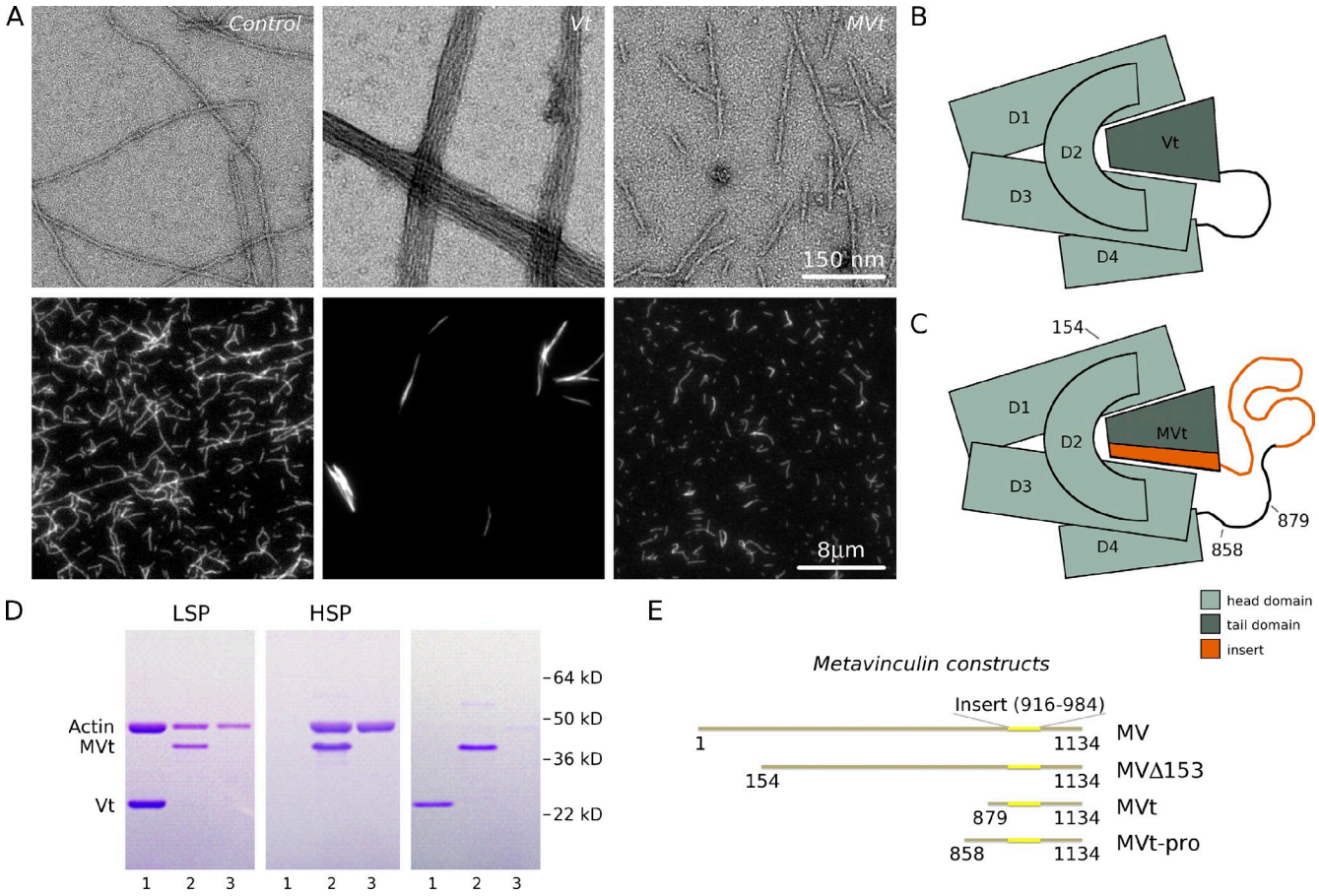

Figure 1. **F-actin organization by Vt and MVt.** (A) Electron (top) and fluorescence microscopy (bottom) images show that actin filaments are organized into bundles by Vt and into short fragments by MVt. (B) Simplified representation of vinculin's domain structure. The tail domain is held pincerlike by the head domain. (C) Simplified representation of MV. H1′ of the MV insert replaces H1 in Vt. Key residues defining the constructs (in E) are marked. (D) Differential pelleting assays confirm actin bundling by Vt (strong bands in the low-speed pellet) and shows actin filament binding of MVt (strong bands in the high-speed pellet). Molar ratio of F-actin to Vt isoform is 1:2. LSP, low-speed pellet; HSP, high-speed pellet; Sup, supernatant. Lane 1: actin + Vt; lane 2: actin + MVt; lane 3: actin. (E) Overview of MV constructs mentioned in the text. The position of the 68-residue insert is marked in yellow. Only the MVt construct starting at residue 879, which lacks the proline-rich region present in MVt-pro, is able to function as an actin-severing protein.

preceding H1 in Vt is replaced by an equivalent ordered region (residues 947–963) in the MV tail domain (MVt, residues 879–1,134). The residues preceding this region in MVt, MV879–946, are largely disordered in the crystal structures. There is little difference between the head–tail interactions of MV and vinculin. Three mutations are found in the insert region that are associated with dilated and hypertrophic cardiomyopathy: Ala934Val, ΔLeu954, and Arg975Trp (Olson et al., 2002), exemplifying the functional importance of the insert region.

Here, we compare the influence of Vt and MVt on actin organization. In previous work, we have shown that Vt binds F-actin and mediates the formation of actin bundles (Janssen et al., 2006). Here, we show that MVt binds and severs actin filaments in a concentration-dependent manner. Unlike Vt, MVt does not bundle actin filaments. 3D reconstructions of actin filaments with bound MVt suggest that the MV879–946 region spatially obscures the vinculin dimerization site, thus preventing higher-order organization of the MVt-bound actin filaments into bundles. These properties of MVt may be essential for modulating compliance of vinculin-induced actin bundles when exposed to rapidly increasing external forces.

Results and discussion

MVt binds actin in a similar orientation as Vt

We determined the structure of actin filaments with bound MVt by EM and 3D image reconstruction. Comparison with previously determined reconstructions of actin with bound Vt (Janssen et al., 2006) shows that the two tail domains bind to actin in a similar manner (Fig. 2 A). Extra density can be clearly identified in the MVt-actin reconstruction (Fig. 2 A, red circle). Because the structures of the Vt and MVt helical bundles are known, the difference between the F-actin–Vt and F-actin–MVt reconstructions allows pinpointing the location of MV879–946 univocally. The location, as would be expected, precedes helix H1′ of MVt when the MVt crystal structure is aligned to the available F-actin–Vt model (Fig. 2 B).

MVt does not induce bundle formation

Vt induces actin bundle formation (Jockusch and Isenberg 1981; Janssen et al., 2006). Although Vt shows a tendency to dimerize in solution under certain conditions, the cryptic

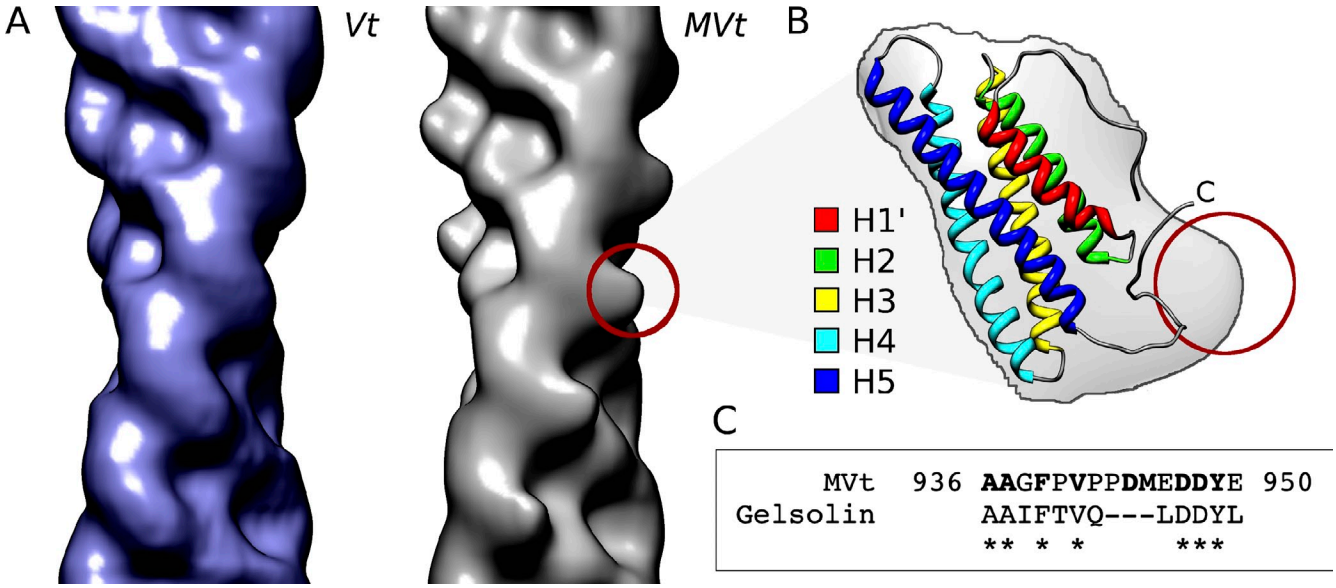

Figure 2. **Structure of actin filaments with bound Vt or MVt.** (A) A comparison between the 3D reconstructions of actin filaments with bound Vt (blue; from Janssen et al., 2006) and F-actin with bound MVt shows that both bind actin filaments in the same orientation and that the only significant difference between the two is an extra density at the base of MVt (red circle). (B) Cartoon representation of the MVt structure (Rangarajan et al., 2010) in the same orientation as the actin-bound MVt marked with the red circle in A. The red circle marks the position of the extra MVt density as in A. An outline of the MVt EM density is shown for reference. Helices H1′ (residues 964–979), H2 (986–1,005), H3 (1,012–1,040), H4 (1,043–1,073), and H5 (1,082–1,114) and the C terminus are highlighted in the structure. Residues 879–946 at the N terminus of MVt are disordered in the available crystal structures. The cryptic actin binding site of Vt is near the C-terminal hairpin between H5 and the C terminus. (C) Sequence alignment of a human gelsolin peptide containing actin-binding sequence AAIVQLDDYL (McLaughlin et al., 1993) and residues 936–950 in the human MVt insert. The sequences are 47% identical. Except for D944 and M945, all conserved residues (bold) in the MVt sequence are identical to the corresponding residues in the aligned gelsolin sequence. Asterisks denote identity between the compared sequences.

dimerization site responsible for actin bundling is a distinctly different region (Abé et al., 2011; Shen et al., 2011). This site only gets exposed when Vt is bound to actin filaments (Johnson and Craig, 2000; Janssen et al., 2006). In contrast to Vt, both fluorescence and EM provide direct evidence that the presence of MVt does not induce actin bundling (Fig. 1 A). Differential pelleting assays support this notion. All of the actin filaments pelleted at low speed when Vt is present, supporting higher-order organization. However, at the low speed step, actin filaments remained in the supernatant in the presence of MVt. In the consecutive step of centrifugation, at high speed, all of the actin filaments pelleted, suggesting that actin remains as single filaments in the presence of MVt (Fig. 1 D).

MVt severs actin filaments

Fluorescence images show that filaments in the presence of MVt are significantly shorter than control actin filaments (Fig. 1 A). Transmission EM of the same samples suggests that, whereas Vt organizes actin filaments into large, highly ordered bundles, the presence of MVt induces short, single actin filaments. We tested whether MVt induces depolymerization of actin filaments by adding increasing amounts of MVt to preformed F-actin. We then checked the supernatants for the presence of G-actin after centrifugation. The fact that we did not detect increases in G-actin concentration in the supernatant (Fig. 3 A, top) indicates that MVt does not induce a significant amount of filament depoly merization. To test for sequestering activity, we added increasing amounts of MVt to G-actin before starting the polymerization process. Because no increase of G-actin in the supernatant was observed (Fig. 3 A, bottom), we conclude that MVt does not retain (sequester) G-actin. These observations indicate that MVt has no significant effect on steady-state filament concentration or filament elongation.

Under these circumstances, the presence of short filaments can be caused by either capping activity at the growing ends or to severing of longer actin filaments. To distinguish between the two possibilities, we used a dual-color elongation assay for testing impediment of filament growth. The results show that filaments in the presence of MVt grow relatively unimpeded (Fig. 3 B), indicating that capping activity at the growing end is not a major contributor to the shortening of the filaments. If severing occurs in the presence of MVt, more filament ends must become available for nucleation. We tested for this effect by using pyrene fluorescence in a polymerization assay. The experiment starts with either F-actin seeds or F-actin–MVt seeds. Adding fresh pyrene-labeled G-actin will result in actin polymerization, which will cause an increase in pyrene fluorescence. The availability of additional filament ends will then result in a higher initial polymerization rate, giving a faster increase in pyrene fluorescence signal. Indeed, the initial polymerization rate in the presence of MVt is significantly higher than in the actin control (Fig. 3 C), indicating that severing does take place.

MVt-severing activity is inversely proportional to its concentration

Using the same pyrene fluorescence assay, we determined the optimal severing concentration to be at a molar ratio of 2:1 for actin/MVt. If less MVt is present (e.g., 6:1), there is only

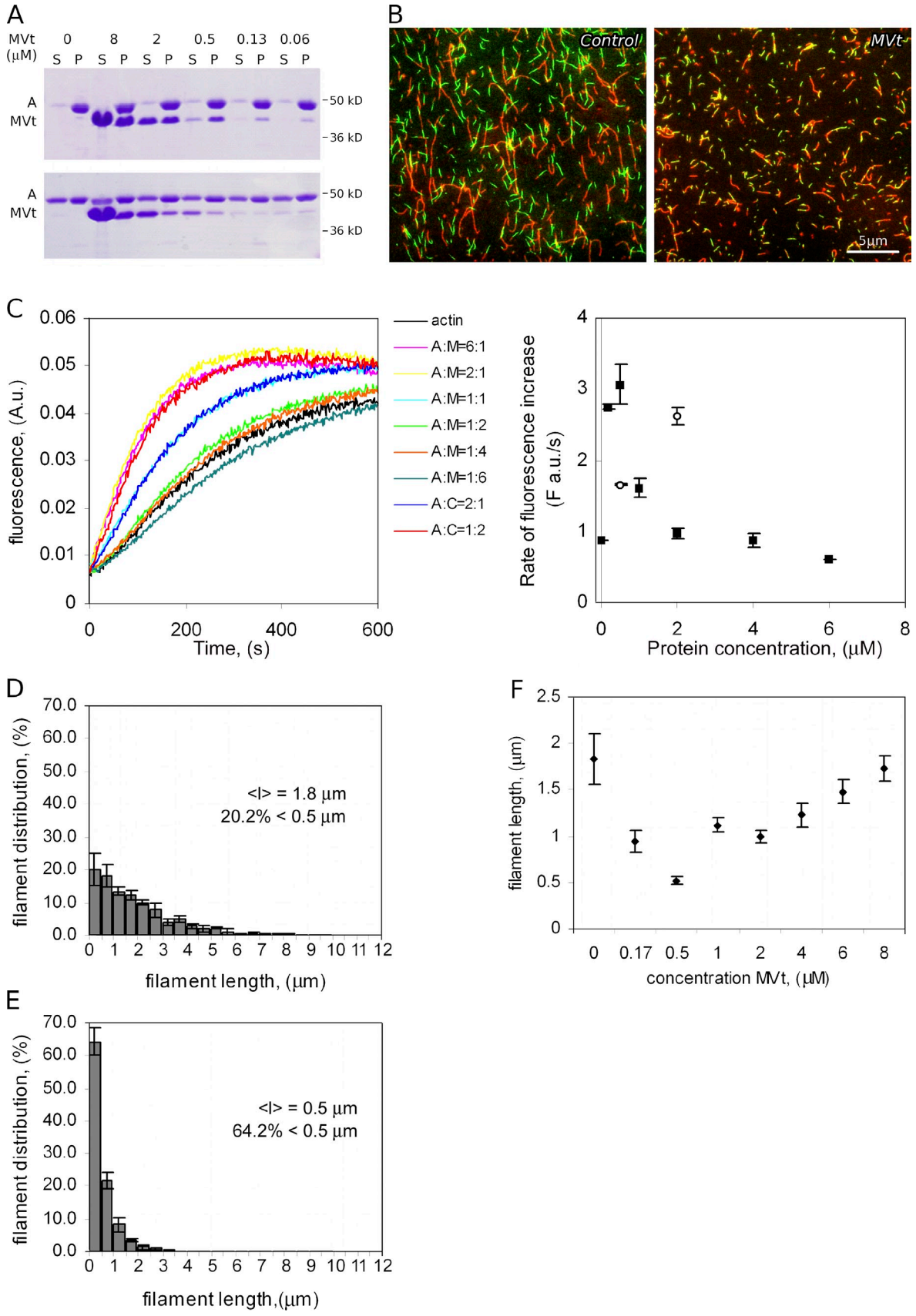

Figure 3. **Effect of MVt on actin filament growth, on the initial actin polymerization rate, and on filament length distribution.** (A) Pelleting assays of actin in the presence of increasing amounts of MVt. (top) Effect of MVt on depolymerization of actin filaments. MVt was added after actin polymerization. The gel shows that no F-actin depolymerization takes place upon MVt increase because there is no increase in actin in the supernatant. (bottom) Effect of MVt

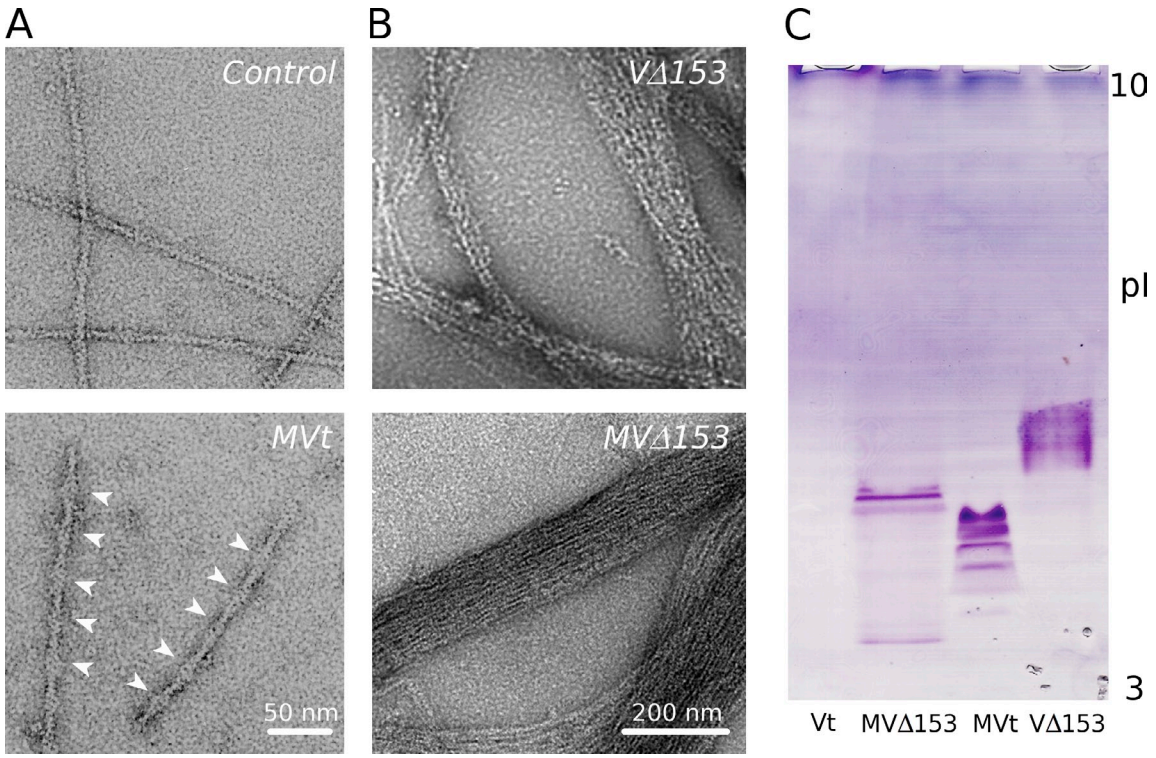

Figure 4. **Actin organization by MVt and MVΔ153.** (A) EM images showing that the severed actin filaments are fully decorated by MVt (arrowheads). (B) Electron micrographs of actin filaments organized by VΔ153 and MVΔ153. Both induce the formation of actin bundles in a similar manner to Vt (see also Fig. 1 A). (C) Isoelectric focusing gel comparing Vt, MVt, MVΔ153, and VΔ153. As expected, Vt does not enter the gel owing to its high isoelectric point of 9.7 (Weekes et al., 1996). MVt is highly acidic, suggesting that many of the acidic residues in the MV879–946 region are fully exposed to the environment. Despite the addition of the acidic head domains, MVΔ153 only has a slightly higher isoelectric point than MVt, only slightly lower than that of VΔ153. These data suggest that the acidic residues in the MV879–946 region are masked in the MVΔ153 construct.

a small penalty in fluorescence increase. However, if successively more MVt is added in the mix, the fluorescence increase gets more and more diminished and eventually drops below the level for bare actin at a ratio of 1:6. The same MVt concentration dependence of the number of filament ends was also directly observed by characterizing the length of actin filaments as a function of MVt concentration (Fig. 3, D and E). Transmission EM shows that MVt is bound to the side of the severed filaments (Fig. 4 A).

The MV insert includes a region that is homologous to the actin-severing region of the gelsolin family

Like cofilin (Andrianantoandro and Pollard, 2006; Pavlov et al., 2007), MVt promotes F-actin severing most efficiently at substoichiometric concentrations. Binding of cofilin induces twist changes and tilting in the filaments (McGough et al., 1997), which is believed to make cofilin-bound actin filaments more fragile and more susceptible to thermal fragmentation than bare filaments (Pfaendtner et al., 2010; McCullough et al., 2011). Efficient severing occurs predominantly at the borders of cofilin-bound and bare segments of the actin filament (Suarez et al., 2011). Unlike cofilin, MVt does not induce changes in actin filament twist, suggesting that it follows an alternative path for severing.

The MV insert contains a 15-residue (936–950) segment that has 47% sequence identity with the actin-binding motif of gelsolin (Fig. 2 C). The sequence contains the DDY motif that is conserved in the severing members in gelsolin family proteins, and replacement of the corresponding residues by DDY in the nonsevering member CapG converts it into a severing protein

on actin monomer sequestering. MVt was added concurrent with actin polymerization. The gel shows that MVt does not sequester actin monomers because an increasing amount of MVt does not retain more G-actin in the supernatant. S, supernatant; P, pellet; A, actin. The lane marked 0 is the actin control. (B) Dual-color fluorescence actin filament elongation assay. New actin (green) grows from the ends of existing (red) actin filaments in the control but also when severed by MVt. Because the same amount of actin was added to both samples, the availability of additional filament ends in the MVt-actin sample will lead to fewer actin monomers added per filament than in the control sample. (C) The initial actin polymerization rate is dependent on the amount of actin filament ends available for nucleation, which in turn is dependent on MVt concentration. Cofilin is used for comparison, and actin alone is used as control (black graph). A, actin; M, MVt; C, cofilin; a.u. arbitrary unit. The quantification on the right shows that the rate of pyrene fluorescence (F) increases as a function of protein concentration. The optimal F-actin severing occurs at a subsaturating MVt concentration. Error bars (SDs) were compiled from independent experiments (closed squares: MVt; open squares: cofilin). (D and E) Quantification of fluorescence microscopy images of actin control (D) and of actin filaments in the presence of MVt at a molar ratio of 2:1 (E) showing that filaments are about four times as short in the presence of MVt if compared with the actin control. (F) Mean filament length as function of MVt concentration. The graph shows that actin filament severing has a biphasic MVt concentration dependency. Error bars represent SDs and were compiled from different experiments. Concentration 0 marks the actin control. <l>, length.

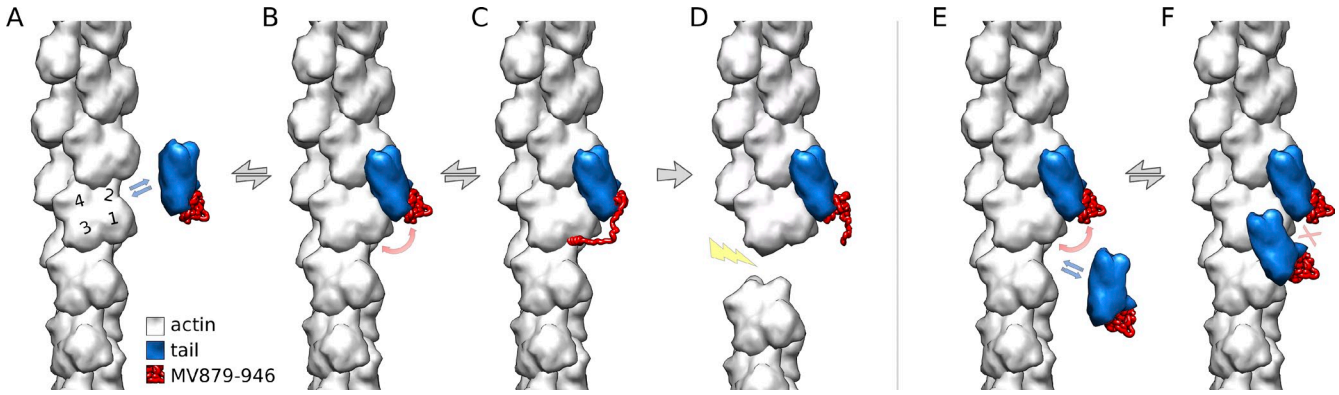

Figure 5. **Cartoon of proposed mechanism for MVt severing and its concentration dependence.** (A) MVt (blue and red) binds to actin filaments in a similar manner as Vt. (B) The MV879–946 region is flexible and can reach the groove between subdomains 1 and 3 of the lower actin filament subunit (red curved double arrow). (C and D) The gelsolin-like motif of the insert can bind in the actin groove and induce severing. (E) If the concentration of MVt is high, a second MVt can bind to the lower actin filament subunit bound to the first MVt. (F) The severing site between subdomains 1 and 3 of the lower actin monomer is no longer accessible for the first MVt.

(Zhang et al., 2006). In gelsolin, the actin-binding motif binds F-actin in the groove between subdomains 1 and 3 (McLaughlin et al., 1993). Marine macrolide toxins bind in the same groove and also induce severing (Klenchin et al., 2003; Allingham et al., 2005), indicating the importance of this site for severing activity. The groove of the barbed-end long-pitch actin neighbor can be easily reached by the flexible region of actin-bound MVt. These facts raise the possibility that MVt residues 936–950 might bind in this groove and induce severing by presenting the DDY motif to actin in a similar manner as gelsolin family members (Fig. 5, A–D). However, if either MVt or Vt occupies the site of a neighboring F-actin subunit, the groove would be masked and not available for binding of the MVt-severing region (Fig. 5, E and F). This scenario would provide an explanation for the concentration dependence of the MVt-severing activity: at substoichiometric concentrations, there is a much higher probability for the MVt-severing region to encounter an available actin groove.

The MV879–946 region spatially occludes the cryptic dimerization site in MVt

The C-terminal tail domain of MV contains a 68-residue insert as well as the actin binding site (Gimona et al., 1988; Janssen et al., 2006). Vt binding to actin promotes local conformational changes in Vt that, in turn, induce formation of large, highly organized actin bundles through opening a cryptic Vt dimerization site. In contrast, we show here that MVt binds, but does not bundle, actin filaments. Furthermore, MVt promotes F-actin severing, most efficiently at substoichiometric concentrations. Despite the replacement of H1 in Vt by H1′ of the MV insert, the binding to actin filaments of the two tail domains appears to be nearly identical as judged by EM reconstructions. Because H1 (or H1′) does not directly participate in actin binding, this is not surprising. In contrast, the location of the MV879–946 region preceding H1′, which is disordered in the MV crystal structure (Rangarajan et al., 2010), is near the cryptic dimerization site identified in vinculin near the C-terminal hairpin (Janssen et al., 2006). Despite the lack of detailed structural knowledge about MV879–946, its location alone provides an explanation for the lack of actin bundling in the presence of MVt: the MV879–946 region spatially occludes the cryptic dimerization sites that are normally exposed in filament-bound Vt.

Longer MV constructs induce actin filament bundle formation and abolish severing

Full-length vinculin, as well as full-length MV, adopts autoinhibited conformations. Vinculin activation exposes, among other sites, the sterically occluded actin-binding regions. To determine the contribution of full-length MV conformation to MVt function, we produced the MV deletion mutant MVΔ153 (Fig. 1 E). This mutant lacks the first 153 N-terminal amino acids, which would otherwise obscure the actin binding sites in the full-length autoinhibited MV. In the context of our study, MVΔ153 is an ideal model for fully activated MV because it is consecutively active to bind actin filaments. In contrast, full-length MV activation in the presence of activating agents, such as one of the talin vinculin binding site regions, might require up to a few hundredfold excess to induce observable actin filament binding. In addition, at those vinculin binding site concentrations, the background significantly interferes with image processing as a result of high background noise in the micrographs. Transmission EM shows unambiguously that MVΔ153 does not sever F-actin but organizes the filaments into bundles similar to those induced by Vt or VΔ153 (Fig. 4 B). Thus, the presence of the residues N terminal of residue 879 abolishes the severing activity of MVt and reinstates bundling activity similar to Vt.

Possible regulation mechanism of MVt bundling and severing activities

Determination of the isoelectric focusing points of Vt, MVt, VΔ153, and MVΔ153 shows that Vt and MVt have significantly different isoelectric points (Fig. 4 C). This difference indicates that many of the charged MV879–946 residues are exposed to the environment. In contrast, VΔ153 and MVΔ153 carry very similar isoelectric points, suggesting that the charged residues in the MV879–946 region that are exposed in MVt are almost entirely masked by the additional domains present in MVΔ153. Together with the difference in severing and bundling behavior

between MVt and MVΔ153, this isoelectric point analysis suggests a possible regulation mechanism that is based on masking and unmasking of the charged residues in the MV879–946 region. Interestingly, a shorter construct (MVt-pro) that contains MVt and the proline-rich region, an additional 21 residues N terminal of MVt (Fig. 1 E), has also been reported to bundle actin filaments in a similar manner to Vt (Witt et al., 2004). This suggests that these 21 residues may be responsible for masking the acidic residues in the MV879–946 region and, thus, potentially regulate the bundling and severing activities of MVt. This is an attractive hypothesis because the proline-rich region contains binding sites for several binding partners of vinculin, including vasodilator-stimulated phosphoprotein, vinexin, and Ponsin (Zamir and Geiger, 2001), suggesting the possibility that other binding partners may be able to regulate MV's severing activity through binding to the proline-rich region. Another attractive possibility is that the masking of the severing site in MV is sensitive to mechanical forces.

Recently, Grashoff et al. (2010) provided direct evidence for vinculin to be intimately linked to focal adhesion mechanosensitivity. The study elegantly shows, using a genetically encoded tension sensor with piconewton sensitivity, that lower fluorescence resonance energy transfer signals (higher tension) occur in instances in which vinculin bears force in the region where the MV insert is located. MV was reported to colocalize with vinculin in vivo (Feramisco et al., 1982; Belkin et al., 1988). It is conceivable that both isoforms work together in complying with sudden changes in tension, both acting as biosensors in cellular force transduction. In this scenario, MV would carry a regulatory role in which its severing activity is activated upon demand when the tension passes some threshold. Application of force would unmask the severing activity of MV, which, in turn, could be relieved once force is diminished. The triggering/unmasking of MV's severing capabilities would provide a very efficient way to locally remodel F-actin in regions where fast reactions to sudden increases in force are needed. Collectively, our data suggest a plausible, but unexpected, regulatory mechanism for MV in which the ability of actin-vinculin assemblies to bear and comply to force is promoted by local disassembly/remodeling of the region under tension.

Materials and methods

Protein preparation

Preparation and storage of actin. Actin was isolated from chicken pectoralis (skeletal muscle) acetone powder (Pardee and Spudich, 1982) and further purified by gel filtration on Sephacryl S-300 in Ca buffer (Amann and Pollard, 2001). It was generally used within 2–3 wk of preparation. 2–4-mg/ml filaments were prepared by polymerization of G-actin into 10 mM imidazole, pH 7.5, 50 mM NaCl, 1 mM $MgCl_2$, 1 mM EDTA, 0.5 mM DTT, and 0.2 mM ATP for 1–2 h at RT or overnight at 4°C.

Cloning, purification, and storage of MV tail. Chicken MVt (residues 879–1,134) was expressed in *Escherichia coli* strain BL21(DE3), and purification was modified from Gimona et al. (1987) as follows: a 40% ammonium sulfate cut was followed by anion exchange chromatography (Q Sepharose HP column; GE Healthcare) and cation exchange chromatography (SP Sepharose HP column; GE Healthcare). Purified protein was dialyzed against 20 mM Tris-HCl, pH 7.5, 150 mM NaCl, and 1 mM EDTA (buffer A) and stored at −80°C until further use. cDNA constructs of full-length MV were provided by R. Liddington (Sanford–Burnham Medical Research Institute, La Jolla, CA) and the Cell Migration Consortium.

Cloning, purification, and storage of MVΔ153. To generate the MVΔ153 construct, chicken MV was truncated at amino acid 153 and preceded by an N-terminal His epitope for affinity chromatography. The absence of errors was confirmed by DNA sequencing. MVΔ153 was expressed in *E. coli* strain BL21(DE3) and purified by affinity chromatography using a Nickel-chelating column (GE Healthcare) followed by anion exchange chromatography (Q Sepharose HP column). The His tag was subsequently removed using biotinylated thrombin (EMD). The protein was stored in buffer A at −80°C until further use.

Cloning, purification, and storage of vinculin tail. Chicken Vt (residues 879–1,066) was expressed in *E. coli* strain TUNER(DE3) (Bakolitsa et al., 1999; Janssen et al., 2006). Cells were amplified until mid–log phase, and protein expression was induced by adding 0.1 mM IPTG for 3 h at 37°C. Cell pellets were frozen at −80°C. Upon thawing, cell pellets were resuspended into 20 mM Tris, pH 7.5, 500 mM NaCl, 5 mM imidazole, 0.1% Tween 20, and 2 mM PMSF before being homogenized (at 10,000–15,000 psi; EmulsiFlex-C3; Avestin). Vt was purified from cleared lysates by affinity chromatography using a Nickel-chelating column. The His tag was cleaved using biotinylated thrombin during a 6-h dialysis at RT in 20 mM Tris, 150 mM NaCl, pH 7.5, and 1 mM DTT. Biotinylated thrombin was captured by streptavidin agarose (EMD) and further dialyzed into the same dialysis buffer. Vt was stored on ice and used within ∼2 d.

Cloning, purification, and storage of VΔ153. Chicken VΔ153 (residues 154–1,066) is a His-tagged construct in pET-15GX (Janssen et al., 2006). Because of its low binding affinity to nickel beads, VΔ153 was recloned into pGEX4T1 Ecor1–Not1 to obtain a GST-tagged construct. VΔ153 was expressed in *E. coli* strain BL21(DE3). Cells were amplified until mid–log phase. Protein expression was induced by 0.1 mM IPTG for 16 h at 15°C. Cell pellets were frozen at −80°C. Upon thawing, pellets were resuspended into PBS, 0.1% Tween 20, one tablet of protease inhibitors with EDTA (Roche), 1 mM DTT, and 2 mM PMSF. Cells were homogenized at 15,000 psi (EmulsiFlex-C3). VΔ153 was purified from cleared cell lysates on a glutathione–Sepharose affinity column (GE Healthcare). The GST tag was cleaved on the column for 3 h at RT using biotinylated thrombin, which was removed using streptavidin agarose. The purified protein was dialyzed against 20 mM Pipes, pH 7.5, 50 mM NaCl, and 1 mM $MgCl_2$ and stored at −80°C until further use.

Biophysical assays

Actin cosedimentation assays. To characterize actin binding and actin bundling by MVt and Vt, a cosedimentation assay was performed using differential centrifugation. G-actin was polymerized in F-actin buffer (10 mM Tris, pH 7.5, 50 mM NaCl, 2 mM DTT, 0.5 mM ATP, and 2 mM $MgCl_2$) for 1 h at RT. MVt or Vt was added to the F-actin in a 2:1 molar ratio and incubated for 45 min on ice. The samples were centrifuged (TLA-100; Beckman Coulter) at low speed (15,434 *g* for 15 min at 4°C) to pellet bundled F-actin, and the supernatant was subsequently centrifuged at high speed (213,483 *g* for 30 min at 4°C) to pellet single actin filaments. Pellets and supernatants were analyzed on 4–20% Tris-glycine gels. The assay was performed in F-actin buffer.

To determine F-actin depolymerization, G-actin was first polymerized in F-actin buffer for 1 h at RT. 4 µM F-actin was then incubated at RT with buffer or increasing amounts of MVt. After 60 min, samples were centrifuged at 312,530 *g* at 4°C for 20 min. Pellets and supernatants were analyzed on 4–20% Tris-glycine gels. To determine G-actin sequestering, 4 µM G-actin was incubated with buffer or increasing amounts of MVt for 15 min at RT. 10× F-actin buffer (500 mM KCl, 10 mM EGTA, 20 mM $MgCl_2$, and 5 mM ATP) was subsequently added, and polymerization was allowed for 60 min at RT. Samples were centrifuged at 312,530 *g* at 4°C for 20 min. Pellets and supernatants were analyzed on 4–20% Tris-glycine gels.

Polymerization fluorescence assay. Unlabeled G-actin and pyrene-labeled G-actin were spun for 1 h at 80 krpm (TLA-100) at 4°C. 1 µM of unlabeled G-actin was polymerized overnight on ice by adding 10× initiation buffer (500 mM KCl, 20 mM $MgCl_2$, 10 mM EGTA, and 5 mM ATP). Cofilin, MVt, or buffer was added in increasing molar ratios to 50 µl of 1-µM F-actin, gently mixed, and incubated for 10 min at RT. These conditions were used as "seeds." For the final reaction G buffer, 1 µM seeds, 1.2 µM of 3.4% pyrene-labeled G-actin, and 20× KME buffer (2 M KCl, 40 mM $MgCl_2$, and 4 mM EGTA) were mixed. Pyrene fluorescence (λ_{ex} = 344 nm and λ_{em} = greater than 385 nm) was measured on a spectrofluorometer using BioKine32 (Jasco). Time between the addition of fresh pyrene–G-actin and the start of fluorometer data collection was estimated at ∼10 s for each measurement.

Isoelectric focusing gel electrophoresis. Vt, MVt, VΔ153, and MVΔ153 were prespinned at 278,100 *g* for 30 min at 4°C and diluted to 0.5 mg/ml. Proteins were diluted twice in 50% glycerol, and 10 µl was loaded on a 3–10-pI isoelectric focusing gel (Criterion; Bio-Rad Laboratories) and run for 1 h at 100 V, 1 h at 250 V, and 30 min at 500 V. The gels have large enough pores to eliminate sieving effects and, thus, are insensitive to molecular weight, accurately recording the isoelectric points of the molecules. Gels were stained using Coomassie gel staining solution (Bio-Rad Laboratories).

EM

EM of actin-VΔ153, actin-MVΔ153, actin-MVt, and actin-Vt assemblies. F-actin was diluted to ∼0.03 mg/ml with 50 mM imidazole, pH 7.0, 100 mM NaCl, 10 mM $MgCl_2$, 10 mM EGTA, 0.5 mM DTT, and 0.2 mM ATP and mixed with VΔ153, MVΔ153, MVt, or Vt. Samples were incubated for 10 min on ice and applied to glow-discharged, 400-mesh copper grids coated with carbon film. The samples were incubated on the grid for 1 min in a humid chamber and then stained with 2% uranyl acetate for 1 min and air dried. Images were recorded with a 1,000 × 1,000 charge-coupled device detector (MultiScan MSC 600HP model 794; Gatan) at RT with an electron microscope (Tecnai G2 T12; FEI Electron Optics) at a nominal magnification of 52,000 at 120 keV and ∼1.5-µm defocus. In parallel to EM experiments, the integrity and folding of the constructs used were verified using SDS gels and differential scanning calorimetry.

EM of actin-MVt assemblies for image reconstruction. Actin filaments decorated with chicken MVt were prepared at 4°C on positively charged lipid layers consisting of a 3:7 wt/wt solution of di-lauryl-phosphatidylinositol and didodecyldimethylammonium bromide dissolved in chloroform (Ward et al., 1990; Taylor and Taylor, 1992; Volkmann et al., 2001). Approximately 0.05 mg/ml monomeric actin was injected through the lipid layer, which was positioned on top of the polymerization buffer (20 mM sodium phosphate buffer, pH 7.0, 50 mM KCl, 1 mM ATP, 2 mM $MgCl_2$, 1 mM EGTA, 1 mM DTT, and ∼0.07 mg/ml MVt). The actin concentration was low enough to grow single actin filaments bound by MVt on lipid layers. Samples were transferred to 200-mesh copper grids coated with lacey carbon films. Specimens were stained with 2% uranyl acetate and air dried. Low-dose images were recorded at RT with an electron microscope (Tecnai G2 T12) at a nominal magnification of 52,000 at 120 keV and ∼1.5-µm defocus (electron dose of ∼10 e^-/A^2). A total of 46 micrographs were recorded on plates (ISO 163; Kodak) and digitized with a scanner (SCAI; Z/I Imaging Corporation) with an effective pixel size of 0.3 nm on the sample.

Image analysis of actin filaments bound by MVt. A hybrid procedure (Volkmann et al., 2005) that combines single-particle reconstruction approaches with helical symmetry (Egelman, 2000) was used to obtain the reconstructions. 14,396 small overlapping segments of actin filaments with bound chicken MVt were selected from the micrographs. The data were then split into two arbitrary halves for independent analysis. This strategy allows cross-validating of features in the reconstructions by comparing between the two subsets (Fig. S1 A). Each subset was phase corrected after fitting of the contrast transfer function with EMAN (Ludtke et al., 1999). An atomic model for unbound actin filaments was used as a starting model for both subsets. For each subset, ∼10 iterations were performed until convergence was achieved.

An analysis of the Fourier shell correlation (FSC) between the reconstructions from the independent half datasets shows that the curve drops below 0.5 ($FSC_{0.5}$), at a resolution of 2.1 nm (Fig. S1 B), indicating that the two reconstructions are indistinguishable at that resolution. Model independence was assured by using actin filament starting models with different helical parameters and also the previously published actin-Vt reconstruction (Janssen et al., 2006). The reconstructions resulting from calculations with these alternative starting models are indistinguishable from the original reconstructions at 2.1 nm according to the corresponding $FSC_{0.5}$.

For both subsets, the actin-MVt density was aligned with the previously determined density of actin-Vt (Janssen et al., 2006) by optimizing the correlation between the two (Volkmann and Hanein, 1999). Difference maps for both subsets between the aligned densities show only one major peak per asymmetric unit. To determine the location of the extra density in respect to MVt and actin, the atomic structure of MVt was aligned with the model of the actin-bound Vt by optimally superimposing the α carbons of the two structures. Although there are differences between the asymmetric units in the MVt crystal structure as well as between the MV and MVt crystals at the atomic level, these differences are below the detection capabilities of the resolution achieved by our EM reconstructions and are thus of little consequence for our interpretations. Sequence analysis to identify the severing motif was performed with CLUSTAL W (Thompson et al., 1994) using the human MV sequence, which is 92% identical to the chicken sequence.

Light microscopy

Image acquisition. Images were acquired using a microscope (Eclipse TE2000-U; Nikon) with Plan Apochromat objective lenses (Nikon) at 100× magnification and a 1.40 oil NA. Image acquisition was performed at RT with F-actin buffer (10 mM Tris, pH 7.5, 50 mM NaCl, 2 mM DTT, 0.5 mM ATP, and 2 mM $MgCl_2$) as an imaging medium. Images were recorded with a charged-coupled device camera (ORCA II-ERG IEEE 1394 model C4742-95-112ERG; Hamamatsu Photonics) using MetaMorph 7.5.2 software (Molecular Devices). Images were post-processed to remove shading effects with the ImageJ (National Institutes of Health) background subtraction routine (ball radius of 25).

Severing assay using fluorescence microscopy. Actin was polymerized for 1 h at RT in F-actin buffer. 2 µM F-actin and increasing ratios of MVt were incubated for 10 min at RT. An equal volume of the fluorochrome Alexa Fluor 488 phalloidin (Invitrogen) in F-actin buffer was added to the mixture in a 1:1 molar ratio with F-actin and incubated for 15 min at RT. The sample was then diluted 50× with H_2O. 5-µl samples were absorbed to 0.01% poly-L-lysine–coated coverslips. Filament length was measured using ImageJ. About six images (two images/three different samples) were analyzed per condition, and all filaments having two distinguishable ends (∼1,200 filaments/condition) were measured.

Dual-color filament elongation assay using fluorescence microscopy. Actin was polymerized for 1 h in F-actin buffer and subsequently incubated with MVt at a molar ratio of 1:2 actin to MVt for 10 min at RT. Rhodamine-labeled phalloidin (Sigma-Aldrich) was added as a fluorochrome in a 1:1 molar ratio to actin and incubated for 10 min on ice. Samples were diluted 10-fold with 0.5 µM Alexa Fluor 488–labeled monomeric actin, incubated for 5 min at RT, and diluted twofold in F-actin buffer. 5-µl samples were absorbed to 0.01% poly-L-lysine–coated coverslips before image acquisition.

Online supplemental material

Fig. S1 shows quality indicators for EM reconstructions. Online supplemental material is available at http://www.jcb.org/cgi/content/full/jcb.201111046/DC1.

We thank Mrs. Larnele Hazelwood for her assistance in the EM sample preparation and screening, Dr. Robert Jeng for supplementary biochemical analysis and lively discussions, Dr. Andrey Bobkov for advice and guidance pertaining to protein purification and biophysical measurements, and Dr. Robert Liddington and the Cell Migration Consortium for providing the cDNA constructs of full-length MV.

This work was supported by the National Institute of General Medical Sciences Cell Migration Consortium grants U54 GM064346 and P01 GM098412 to D. Hanein and N. Volkmann.

Submitted: 9 November 2011
Accepted: 17 April 2012

References

Abé, C., F. Dietrich, P. Gajula, M. Benz, K.-P. Vogel, M. van Gastel, S. Illenberger, W.H. Ziegler, and H.-J. Steinhoff. 2011. Monomeric and dimeric conformation of the vinculin tail five-helix bundle in solution studied by EPR spectroscopy. *Biophys. J.* 101:1772–1780. http://dx.doi.org/10.1016/j.bpj.2011.08.048

Allingham, J.S., A. Zampella, M.V. D'Auria, and I. Rayment. 2005. Structures of microfilament destabilizing toxins bound to actin provide insight into toxin design and activity. *Proc. Natl. Acad. Sci. USA*. 102:14527–14532. http://dx.doi.org/10.1073/pnas.0502089102

Amann, K.J., and T.D. Pollard. 2001. The Arp2/3 complex nucleates actin filament branches from the sides of pre-existing filaments. *Nat. Cell Biol.* 3:306–310. http://dx.doi.org/10.1038/35060104

Andrianantoandro, E., and T.D. Pollard. 2006. Mechanism of actin filament turnover by severing and nucleation at different concentrations of ADF/cofilin. *Mol. Cell*. 24:13–23. http://dx.doi.org/10.1016/j.molcel.2006.08.006

Bakolitsa, C., J.M. de Pereda, C.R. Bagshaw, D.R. Critchley, and R.C. Liddington. 1999. Crystal structure of the vinculin tail suggests a pathway for activation. *Cell*. 99:603–613. http://dx.doi.org/10.1016/S0092-8674(00)81549-4

Bakolitsa, C., D.M. Cohen, L.A. Bankston, A.A. Bobkov, G.W. Cadwell, L. Jennings, D.R. Critchley, S.W. Craig, and R.C. Liddington. 2004. Structural basis for vinculin activation at sites of cell adhesion. *Nature*. 430:583–586. http://dx.doi.org/10.1038/nature02610

Belkin, A.M., O.I. Ornatsky, A.E. Kabakov, M.A. Glukhova, and V.E. Koteliansky. 1988. Diversity of vinculin/meta-vinculin in human tissues and cultivated cells. Expression of muscle specific variants of vinculin in human aorta smooth muscle cells. *J. Biol. Chem.* 263:6631–6635.

Borgon, R.A., C. Vonrhein, G. Bricogne, P.R. Bois, and T. Izard. 2004. Crystal structure of human vinculin. *Structure*. 12:1189–1197. http://dx.doi.org/10.1016/j.str.2004.05.009

Byrne, B.J., Y.J. Kaczorowski, M.D. Coutu, and S.W. Craig. 1992. Chicken vinculin and meta-vinculin are derived from a single gene by alternative splicing of a 207-base pair exon unique to meta-vinculin. *J. Biol. Chem.* 267:12845–12850.

Egelman, E.H. 2000. A robust algorithm for the reconstruction of helical filaments using single-particle methods. *Ultramicroscopy*. 85:225–234. http://dx.doi.org/10.1016/S0304-3991(00)00062-0

Feramisco, J.R., J.E. Smart, K. Burridge, D.M. Helfman, and G.P. Thomas. 1982. Co-existence of vinculin and a vinculin-like protein of higher molecular weight in smooth muscle. *J. Biol. Chem.* 257:11024–11031.

Gimona, M., D.O. Fürst, and J.V. Small. 1987. Metavinculin and vinculin from mammalian smooth muscle: bulk isolation and characterization. *J. Muscle Res. Cell Motil.* 8:329–341. http://dx.doi.org/10.1007/BF01568889

Gimona, M., J.V. Small, M. Moeremans, J. Van Damme, M. Puype, and J. Vandekerckhove. 1988. Porcine vinculin and metavinculin differ by a 68-residue insert located close to the carboxy-terminal part of the molecule. *EMBO J.* 7:2329–2334.

Glukhova, M.A., A.E. Kabakov, A.M. Belkin, M.G. Frid, O.I. Ornatsky, N.I. Zhidkova, and V.E. Koteliansky. 1986. Meta-vinculin distribution in adult human tissues and cultured cells. *FEBS Lett.* 207:139–141. http://dx.doi.org/10.1016/0014-5793(86)80027-8

Golji, J., and M.R.K. Mofrad. 2010. A molecular dynamics investigation of vinculin activation. *Biophys. J.* 99:1073–1081. http://dx.doi.org/10.1016/j.bpj.2010.05.024

Grashoff, C., B.D. Hoffman, M.D. Brenner, R. Zhou, M. Parsons, M.T. Yang, M.A. McLean, S.G. Sligar, C.S. Chen, T. Ha, and M.A. Schwartz. 2010. Measuring mechanical tension across vinculin reveals regulation of focal adhesion dynamics. *Nature*. 466:263–266. http://dx.doi.org/10.1038/nature09198

Izard, T., G. Evans, R.A. Borgon, C.L. Rush, G. Bricogne, and P.R. Bois. 2004. Vinculin activation by talin through helical bundle conversion. *Nature*. 427:171–175. http://dx.doi.org/10.1038/nature02281

Janssen, M.E., E. Kim, H. Liu, L.M. Fujimoto, A. Bobkov, N. Volkmann, and D. Hanein. 2006. Three-dimensional structure of vinculin bound to actin filaments. *Mol. Cell*. 21:271–281. http://dx.doi.org/10.1016/j.molcel.2005.11.020

Jockusch, B.M., and G. Isenberg. 1981. Interaction of alpha-actinin and vinculin with actin: opposite effects on filament network formation. *Proc. Natl. Acad. Sci. USA*. 78:3005–3009. http://dx.doi.org/10.1073/pnas.78.5.3005

Johnson, R.P., and S.W. Craig. 2000. Actin activates a cryptic dimerization potential of the vinculin tail domain. *J. Biol. Chem.* 275:95–105. http://dx.doi.org/10.1074/jbc.275.1.95

Klenchin, V.A., J.S. Allingham, R. King, J. Tanaka, G. Marriott, and I. Rayment. 2003. Trisoxazole macrolide toxins mimic the binding of actin-capping proteins to actin. *Nat. Struct. Biol.* 10:1058–1063. http://dx.doi.org/10.1038/nsb1006

Koteliansky, V.E., A.M. Belkin, M.G. Frid, and M.A. Glukhova. 1991. Developmental changes in expression of adhesion-mediating proteins in human aortic smooth muscle. *Biochem. Soc. Trans.* 19:1072–1076.

Ludtke, S.J., P.R. Baldwin, and W. Chiu. 1999. EMAN: semiautomated software for high-resolution single-particle reconstructions. *J. Struct. Biol.* 128:82–97. http://dx.doi.org/10.1006/jsbi.1999.4174

McCullough, B.R., E.E. Grintsevich, C.K. Chen, H. Kang, A.L. Hutchison, A. Henn, W. Cao, C. Suarez, J.L. Martiel, L. Blanchoin, et al. 2011. Cofilin-linked changes in actin filament flexibility promote severing. *Biophys. J.* 101:151–159. http://dx.doi.org/10.1016/j.bpj.2011.05.049

McGough, A., B. Pope, W. Chiu, and A. Weeds. 1997. Cofilin changes the twist of F-actin: implications for actin filament dynamics and cellular function. *J. Cell Biol.* 138:771–781. http://dx.doi.org/10.1083/jcb.138.4.771

McLaughlin, P.J., J.T. Gooch, H.G. Mannherz, and A.G. Weeds. 1993. Structure of gelsolin segment 1-actin complex and the mechanism of filament severing. *Nature*. 364:685–692. http://dx.doi.org/10.1038/364685a0

Olson, T.M., S. Illenberger, N.Y. Kishimoto, S. Huttelmaier, M.T. Keating, and B.M. Jockusch. 2002. Metavinculin mutations alter actin interaction in dilated cardiomyopathy. *Circulation*. 105:431–437. http://dx.doi.org/10.1161/hc0402.102930

Pardee, J.D., and J.A. Spudich. 1982. Mechanism of K^+-induced actin assembly. *J. Cell Biol.* 93:648–654. http://dx.doi.org/10.1083/jcb.93.3.648

Pavlov, D., A. Muhlrad, J. Cooper, M. Wear, and E. Reisler. 2007. Actin filament severing by cofilin. *J. Mol. Biol.* 365:1350–1358. http://dx.doi.org/10.1016/j.jmb.2006.10.102

Pfaendtner, J., E.M. De La Cruz, and G.A. Voth. 2010. Actin filament remodeling by actin depolymerization factor/cofilin. *Proc. Natl. Acad. Sci. USA*. 107:7299–7304. http://dx.doi.org/10.1073/pnas.0911675107

Rangarajan, E.S., J.H. Lee, S.D. Yogesha, and T. Izard. 2010. A helix replacement mechanism directs metavinculin functions. *PLoS ONE*. 5:e10679. http://dx.doi.org/10.1371/journal.pone.0010679

Saga, S., M. Hamaguchi, M. Hoshino, and K. Kojima. 1985. Expression of meta-vinculin associated with differentiation of chicken embryonal muscle cells. *Exp. Cell Res.* 156:45–56. http://dx.doi.org/10.1016/0014-4827(85)90260-5

Shen, K., C.E. Tolbert, C. Guilluy, V.S. Swaminathan, M.E. Berginski, K. Burridge, R. Superfine, and S.L. Campbell. 2011. The vinculin C-terminal hairpin mediates F-actin bundle formation, focal adhesion, and cell mechanical properties. *J. Biol. Chem.* 286:45103–45115. http://dx.doi.org/10.1074/jbc.M111.244293

Suarez, C., J. Roland, R. Boujemaa-Paterski, H. Kang, B.R. McCullough, A.-C. Reymann, C. Guérin, J.-L. Martiel, E.M. De la Cruz, and L. Blanchoin. 2011. Cofilin tunes the nucleotide state of actin filaments and severs at bare and decorated segment boundaries. *Curr. Biol.* 21:862–868. http://dx.doi.org/10.1016/j.cub.2011.03.064

Taylor, K.A., and D.W. Taylor. 1992. Formation of 2-D paracrystals of F-actin on phospholipid layers mixed with quaternary ammonium surfactants. *J. Struct. Biol.* 108:140–147. http://dx.doi.org/10.1016/1047-8477(92)90013-Z

Thompson, J.D., D.G. Higgins, and T.J. Gibson. 1994. CLUSTAL W: improving the sensitivity of progressive multiple sequence alignment through sequence weighting, position-specific gap penalties and weight matrix choice. *Nucleic Acids Res.* 22:4673–4680. http://dx.doi.org/10.1093/nar/22.22.4673

Turner, C.E., and K. Burridge. 1989. Detection of metavinculin in human platelets using a modified talin overlay assay. *Eur. J. Cell Biol.* 49:202–206.

Volkmann, N., and D. Hanein. 1999. Quantitative fitting of atomic models into observed densities derived by electron microscopy. *J. Struct. Biol.* 125:176–184. http://dx.doi.org/10.1006/jsbi.1998.4074

Volkmann, N., K.J. Amann, S. Stoilova-McPhie, C. Egile, D.C. Winter, L. Hazelwood, J.E. Heuser, R. Li, T.D. Pollard, and D. Hanein. 2001. Structure of Arp2/3 complex in its activated state and in actin filament branch junctions. *Science*. 293:2456–2459. http://dx.doi.org/10.1126/science.1063025

Volkmann, N., H. Liu, L. Hazelwood, E.B. Krementsova, S. Lowey, K.M. Trybus, and D. Hanein. 2005. The structural basis of myosin V processive movement as revealed by electron cryomicroscopy. *Mol. Cell*. 19:595–605. http://dx.doi.org/10.1016/j.molcel.2005.07.015

Ward, R.J., J.F. Menetret, F. Pattus, and K. Leonard. 1990. Method for forming two-dimensional paracrystals of biological filaments on lipid monolayers. *J. Electron Microsc. Tech.* 14:335–341. http://dx.doi.org/10.1002/jemt.1060140408

Weekes, J., S.T. Barry, and D.R. Critchley. 1996. Acidic phospholipids inhibit the intramolecular association between the N- and C-terminal regions of vinculin, exposing actin-binding and protein kinase C phosphorylation sites. *Biochem. J.* 314:827–832.

Witt, S., A. Zieseniss, U. Fock, B.M. Jockusch, and S. Illenberger. 2004. Comparative biochemical analysis suggests that vinculin and metavinculin cooperate in muscular adhesion sites. *J. Biol. Chem.* 279:31533–31543. http://dx.doi.org/10.1074/jbc.M314245200

Xu, W., H. Baribault, and E.D. Adamson. 1998. Vinculin knockout results in heart and brain defects during embryonic development. *Development*. 125:327–337.

Zamir, E., and B. Geiger. 2001. Molecular complexity and dynamics of cell-matrix adhesions. *J. Cell Sci.* 114:3583–3590.

Zemljic-Harpf, A.E., J.C. Miller, S.A. Henderson, A.T. Wright, A.M. Manso, L. Elsherif, N.D. Dalton, A.K. Thor, G.A. Perkins, A.D. McCulloch, and R.S. Ross. 2007. Cardiac-myocyte-specific excision of the vinculin gene disrupts cellular junctions, causing sudden death or dilated cardiomyopathy. *Mol. Cell. Biol.* 27:7522–7537. http://dx.doi.org/10.1128/MCB.00728-07

Zhang, Y., S.M. Vorobiev, B.G. Gibson, B. Hao, G.S. Sidhu, V.S. Mishra, E.G. Yarmola, M.R. Bubb, S.C. Almo, and F.S. Southwick. 2006. A CapG gain-of-function mutant reveals critical structural and functional determinants for actin filament severing. *EMBO J.* 25:4458–4467. http://dx.doi.org/10.1038/sj.emboj.7601323

Ziegler, W.H., R.C. Liddington, and D.R. Critchley. 2006. The structure and regulation of vinculin. *Trends Cell Biol.* 16:453–460. http://dx.doi.org/10.1016/j.tcb.2006.07.004